Thèse de doctorat

NNT : ***

n°LAL : ***

Study of ^{208}Tl background rejection influence on the $0\nu\beta\beta$ decay sensitivity Characterisation of SuperNEMO demonstrator calorimeter timing performance

Thèse de doctorat de l'Université Paris-Saclay
préparée à l'Université Paris Saclay au sein du Laboratoire Irène-Joliot Curie
(anciennement Laboratoire de l'Accélérateur Linéaire)

École doctorale n°576 Particles, Hadrons, Energy, Nuclei,
Instrumentation, Imaging, Cosmos et Simulation (PHENIICS)
Spécialité de doctorat : Physique des particules

Thèse présentée et soutenue à Orsay, le 11 décembre 2020, par

CLOÉ GIRARD-CARILLO

Composition du Jury :

Alessandra Tonazzo APC - Paris	Rapporteure
Mark C. Chen Queen's University	Rapporteur
Christine Marquet CENBG - Bordeaux-Gradignan	Examinatrice
Achille Stocchi LAL - Orsay	Examinateur
Laurent Simard LAL - Orsay	Directeur de thèse
Mathieu Bongrand LAL - Orsay	Co-directeur de thèse

Contents

Chapter 1

Phenomenology of particle physics and experimental status

The idea that our universe is composed of very small and indivisible particles is not new, and has its origins in various cultures. The word *atom*, which is derived from the Greek word *atomos*, also means *unbreakable*. Currently, the theory that brings together our understanding of matter, the *elementary particles*, and its interactions, the *forces*, is called the Standard Model of Particle Physics (SM). This model provides a unified picture where the forces between particles are themselves described by the exchange of particles. Remarkably, the Standard Model succeeds in describing most current experimental data and represents one of the triumph of modern physics. A brief review of this model is given in the first part of this chapter.

Nevertheless, some questions are still open, for which the SM does not provide answers, as the matter/antimatter asymmetry of the universe, the dark matter nature and the origin of neutrino masses. In order to account for these observational discrepancies, new physics models have to be investigated. If a satisfactory theory beyond the Standard Model emerges, it could greatly impact our comprehension of the fundamental mechanisms of the Universe. In particular, the third one, concerning the mass of neutrinos, is the one which ultimately motivated this PhD, and is therefore particularly described in the second part of this chapter. It could also have an impact on the comprehension of matter/antimatter asymmetry origin. The third part of this chapter aims at giving an overview of the current research of a non-standard decay, of which the detector I worked on is a part.

1.1 The Standard Model of particle physics

The Standard Model of particle physics describes the strong, weak and electromagnetic interactions, gauged by the symmetry group $SU(3)_C \times SU(2)_L \times U(1)_Y$, where C represents the colour, L the left-handed chirality and Y the hypercharge. The SM gauge bosons (the 8 gluons, Z_0, $W^{\pm}$ and the photon) mediate these interactions. The scalar Higgs field is at the origin of electroweak symmetry

breaking (i.e. $SU(2)_L \times U(1)_Y \rightarrow U(1)_{em}$), and is responsible for giving masses to elementary particles.

1.1.1 Particle content

The particle content is presented in Fig. 1.1.

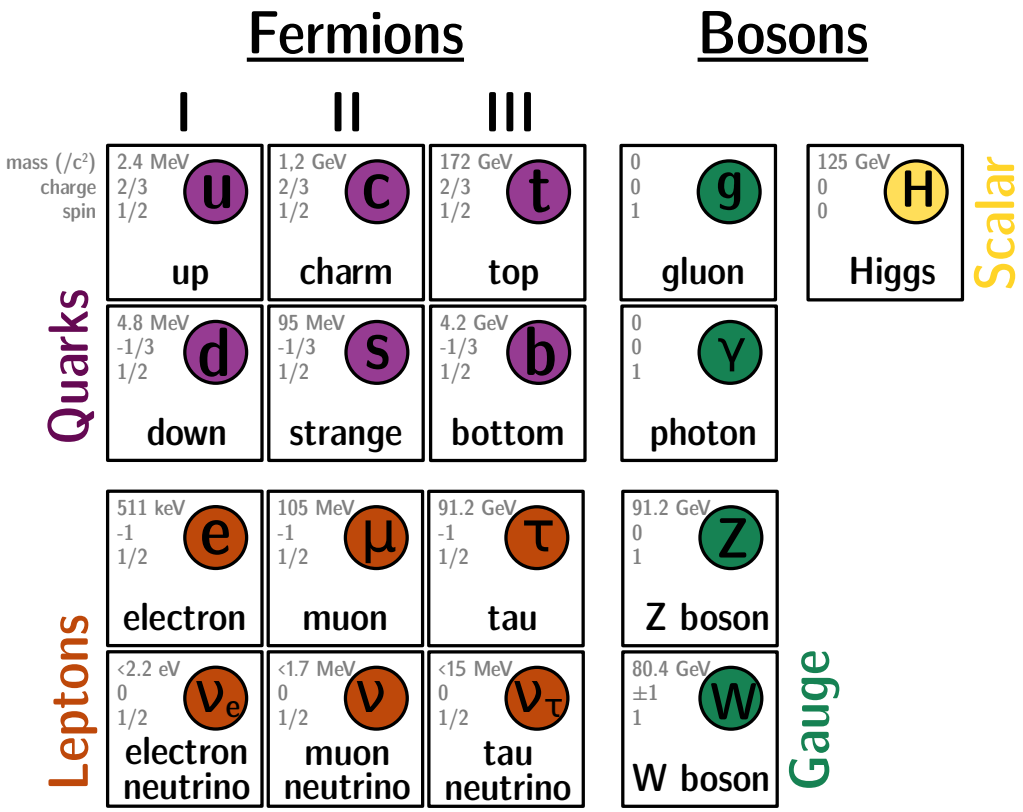

Figure 1.1: The Standard Model of elementary particles.

Fermions

Fermions are particles with half-integer spins, obeying to the Pauli exclusion principle. The properties of the 12 fermions of the Standard Model allow to classify them into categories, according to the forces to which they are sensitive. All fermions experience the weak force, while only 9 of them participate in the electromagnetic interaction of QED, the neutrinos being electrically neutral. Only quarks feel the strong force, as they are the only ones carrying the QCD charge. The SM fermions are further classified in three generations.

To construct the electroweak $SU(2)_L \times U(1)_Y$ theory, the fermions field can be represented through their chirality properties. For one given generation, the left-

handed chiral components of the fermion fields are grouped into $SU(2)$ doublets

$$L_L = \begin{pmatrix} \nu_L \\ l_L \end{pmatrix} \qquad \text{and} \qquad q_L = \begin{pmatrix} u_L \\ d_L \end{pmatrix} , \tag{1.1}$$

where L_L stands for the leptons and q_L for the quarks. The right-handed components of the other fermions are $SU(2)$ singlets, e_R, u_R and d_R. In the SM, neutrinos are assumed to have only left-handed components. The generalisation for three generations is not presented in this chapter.

Bosons

Bosons are particles with integer spins, described by the Bose-Einstein statistics. The elementary bosons of the SM, also called gauge bosons, have a spin 1 and mediate the interaction between elementary particles. The Higgs boson, with a spin 0, is a scalar boson.

1.1.2 Where the Standard Model ends

An ultimate Model of particle physics should theoretically predict and explain all particle masses and interactions, with few free parameters. Despite the success of the Standard Model in the explanation of particle behaviours, unanswered questions remain.

- Matter/antimatter asymmetry
  The beginning of the Universe should have produced the same quantity of matter and antimatter, simply because nor matter nor antimatter should be advantaged over the other. Nevertheless, from experimental evidences, we know that the former dominates over the latter. This is known as the Baryonic Asymmetry of the Universe (BAU). The amount of charge-parity (CP) violation observed in the quark sector being not sufficient to explain this asymmetry, the SM fails to explain this unbalance.

- Dark matter
  The known matter described by the SM represents only 5% of the Universe composition. Another 27% represents matter existing in a *non-luminous* form, called Dark Matter (DM), for which the Standard Model does not provide a viable candidate. Such matter is colourless and electrically neutral, and can only have weak and/or gravitational interactions. Early evidence for the existence of DM was provided by galaxy rotation curves: relying only on *luminous* matter, the velocity should decrease as $r^{-1/2}$, where r is the distance to the galaxy centre. This is in disagreement with observation, suggesting the existence of additional matter. The remaining 68% of the universe composition is dark energy, an unknown form of energy introduced, among others, to explain the accelerated expansion of the universe.

- Neutrino masses
  Providing an explanation to neutrino masses, and understanding their

smallness compared to other fermions, is an important question in modern particle physics. First proposed by Fermi in 1933 [1], neutrinos were believed to be mass-less, and in its original formulation, the SM included no neutrino mass term. Neutrino oscillations, which are confirmed by a plethora of experiments, provided evidence for neutrino masses. Given their unique neutral character, neutrinos can be either Dirac (particles and anti-particles are distinct) or Majorana (particles are their own anti-particles) fermions. Looking for neutrinoless beta decays is one of the preferred ways to probe the Majorana nature of neutrinos.

This is a non-exhaustive list, and other tensions exist between theory and observation, such as the anomalous magnetic moment of the muon, or the flavour universality violation in B and D meson decays.

1.2 Going beyond the Standard Model with neutrinos

1.2.1 Neutrino flavors and oscillations

The neutrinos are only detected through their weak interaction with matter, which defines the three neutrino flavours. For instance, an electron neutrino ν_e is defined through a charged-current weak interaction of an electron. In the same manner, the charged-current weak interaction of an electron neutrino produces an electron.

The first (and only) evidence that neutrinos are massive is the observation of neutrino oscillations, first predicted in 1957 by Pontecorvo [2]. In 1998 emerged from the Super-Kamiokande experiment the confirmation for neutrino flavour changing: the deficit of muon neutrinos was inconsistent with expectations based on calculations of the atmospheric neutrino flux, suggesting that muon neutrinos oscillate with tau neutrinos [3].

Flavour and mass eigenstates

The neutrino oscillation is a quantum-mechanical effect, which can be understood in terms of the relationship between the three weak interaction eigenstates, ν_e, ν_μ and ν_τ that can be experimentally measured, and the three mass eigenstates, ν_1, ν_2 and ν_3, that propagate in space-time. If the neutrino mass is zero thus, in the charged lepton sector, a basis can always be defined such as the lepton mass matrix is diagonal. However, by introducing even small masses for the neutrinos, a common basis were the two lepton mass matrix are diagonal can't be found. The neutrino interaction and mass eigenstate are related by the U_{PMNS} matrix such as

$$\begin{pmatrix} \nu_e \\ \nu_\mu \\ \nu_\tau \end{pmatrix} = \begin{pmatrix} U_{e1} & U_{e2} & U_{e3} \\ U_{\mu 1} & U_{\mu 2} & U_{\mu 3} \\ U_{\tau 1} & U_{\tau 2} & U_{\tau 3} \end{pmatrix} \begin{pmatrix} \nu_1 \\ \nu_2 \\ \nu_3 \end{pmatrix} , \tag{1.2}$$

where U_{e2} denotes the ν_2-component of the interaction eigenstate ν_e, for instance.

Oscillation probability

Considering two-flavour neutrino ν_α and ν_β, the oscillation probability is written as

$$\mathcal{P}_{\nu_\alpha \to \nu_\beta}(t) = \sin^2(2\theta)\sin^2\left(\frac{\Delta m^2}{4E}L\right) \qquad (\nu_\alpha \neq \nu_\beta) \tag{1.3}$$

where L is the source-detector distance, E is the neutrino energy and θ is the mixing angle with a value in the interval $0 \leq \theta \leq \pi/2$. In the particular case of two-neutrino mixing the squared mass difference Δm^2 is defined as

$$\Delta m^2 = \Delta m^2_{12} = m_2^2 - m_1^2\,, \tag{1.4}$$

where m_1 and m_2 are the masses of the states ν_1 and ν_2 defined as $m_1 < m_2$ so that $\Delta m^2 > 0$. The first observation coming with Eq. (1.3) is that if neutrino masses were not degenerated, oscillations would not be possible. A direct consequence of this statement is that if neutrinos are mass-less, they cannot oscillate. Then, we only need two non-zero neutrino masses for neutrino oscillation to be observed.

Neutrino mixing is a quantum effect: an interaction state ν_α is produced in a well-determined state, which is a linear combination of the three mass eigenstates. When the neutrino propagates through space-time, these coefficient are free to evolve as long as the neutrino is not detected and therefore measured. The neutrino is then no more determined as ν_α. When the neutrino is detected, an eigenstate is determined in the interaction basis, corresponding to ν_e, ν_μ or ν_τ. Thus ν_α can be measured as another neutrino state, with the probability given in Eq. (1.3).

Neutrinos mass ordering

The sensitivity to Δm^2 of an experiment is the value of Δm^2 for which $\Delta m^2 L/2E \sim 1$, allowing to classify neutrino experiments.

Atmospheric neutrinos are created by the interaction between the cosmic rays and the nuclei in the earth's atmosphere: protons of the cosmic rays interact with atmospheric nuclei, mostly producing pions. Pions mainly decay into muons and muon neutrinos in the energy range of $[0.5 - 10^2]$ GeV. Atmospheric neutrino experiments, with a source-detector distance about 10^4 km, are then sensitive to $\Delta m^2 \sim 10^{-4}$ eV^2, above the order of magnitude of Δm^2_{32} , which allow to rename $\Delta m^2_{32} = \Delta m^2_{atm}$.

In nuclear fusion processes, protons are transformed into neutrons through a weak process, producing electron neutrinos with an energy about $[0.2 - 15]$ MeV. Since the sun-earth distance is about 1.5×10^{11} km, solar neutrino experiments are sensitive to $\Delta m^2 \sim 10^{-12}$ eV^2. Comparing this sensitivity with Δm^2_{12}, one can write $\Delta m^2_{12} = \Delta m^2_{sol}$. The study of neutrino mixing allows us to have access to precise values of squared mass differences Δm^2_{sol} and Δm^2_{atm}.

Thanks to matter effects in the Sun, we know that $\Delta m^2_{sol} > 0$. Since Δm^2_{atm} is essentially measured via neutrino oscillations in vacuum, which exclusively depend on its absolute value, its sign is unknown at the moment. Therefore, the neutrino masses can be ordered in two ways: normal ordering (NO) if $\Delta m^2_{atm} > 0$ and inverted ordering (IO) if $\Delta m^2_{atm} > 0$. Both orderings are presented in Fig. 1.2.

Indirect constraints may come from the observation of the neutrinoless double beta decay or from cosmological bounds on the sum of the neutrino masses.

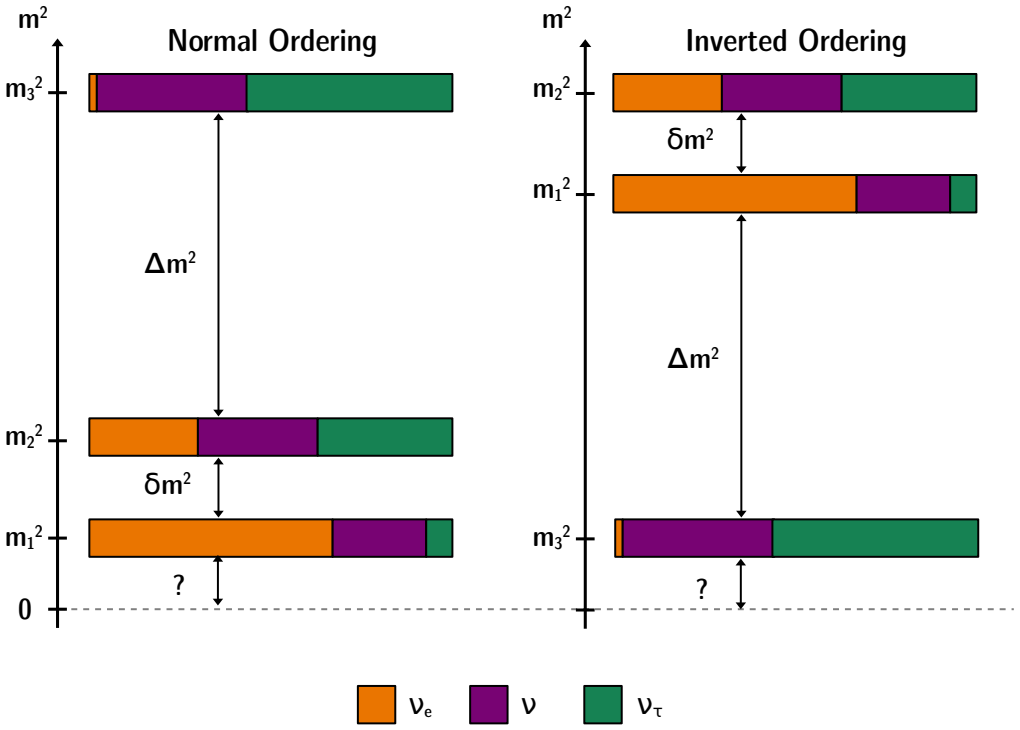

Figure 1.2: Graphic view of the probability of finding one of the flavor eigenstates if the neutrino is in a certain mass eigenstate. Normal and inverted orderings are presented. $\delta m^2 = m_2^2 - m_1^2$ and $\Delta m^2 = m_3^2 - (m_1^2 + m_2^2)/2$.

Oscillation data

The leptonic mixing matrix defined in Eq. (1.2) can be parameterised as

$$U_{PMNS} = \begin{pmatrix} c_{12}c_{13} & s_{12}c_{13} & s_{13}e^{-i\delta_{CP}} \\ -s_{12}c_{23} - c_{12}s_{23}s_{13}e^{i\delta_{CP}} & c_{12}c_{23} - s_{12}s_{23}s_{13}e^{i\delta_{CP}} & s_{23}c_{13} \\ s_{12}s_{23} - c_{12}c_{23}s_{13}e^{i\delta_{CP}} & -c_{12}s_{23} - s_{12}c_{23}s_{13}e^{i\delta_{CP}} & c_{23}c_{13} \end{pmatrix} \quad (1.5)$$

where $c_{ij} = \cos\theta_{ij}$, $s_{ij} = \sin\theta_{ij}$ and δ_{CP} is the Dirac CP violating phase. Tab. 1.1 sums up the latest best fit values of U_{PMNS} parameters [4].

Fig. 1.3 pictures the relative different contributions of quark and neutrino matrix elements. Unlike the CKM matrix for the quark sector, the neutrino mixing angles are found to be large.

1.2.2 Neutrino masses and nature

As neutrinos are neutral particles, several mass terms can be introduced in the SM Lagrangian, depending on their nature.

Parameter	Hierarchy	Best fit
Δm^2_{12} (10^{-5}eV^2)	NO or IO	7.37
$\sin^2\theta_{12}$ (10^{-1})	NO or IO	2.97
Δm^2 (10^{-3}eV^2)	NO	2.52
Δm^2 (10^{-3}eV^2)	IO	2.50
$\sin^2\theta_{13}$ (10^{-2})	NO	2.15
$\sin^2\theta_{13}$ (10^{-2})	IO	2.15
$\sin^2\theta_{23}$ (10^{-1})	NO	4.22
$\sin^2\theta_{23}$ (10^{-1})	IO	5.90
δ_{CP}/π	NO	1.40
δ_{CP}/π	IO	1.30

Table 1.1: Best fit values of neutrino oscillation parameters, for inverted and normal orderings (IO and NO, respectively) [4]. $\Delta m^2 = m_3^2 - (m_1^2 + m_2^2)/2$ with $+\Delta m$ for IO. The CP violating phase is taken in the interval $0 \leq \delta_{CP}/\pi \leq 2$.

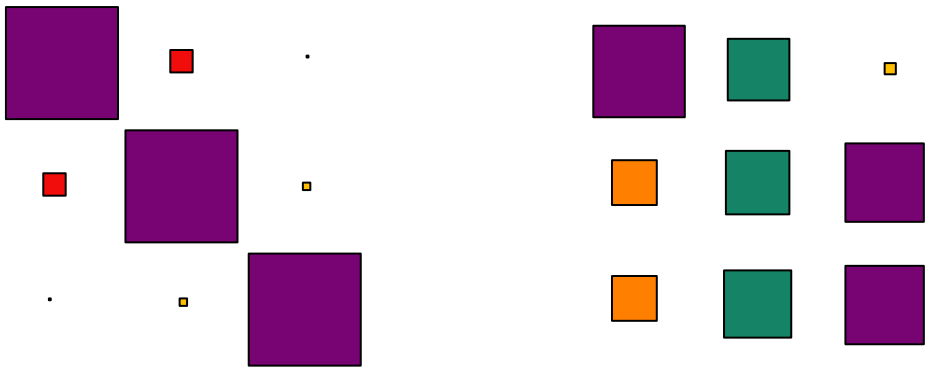

(a) CKM matrix. (b) PMNS matrix.

Figure 1.3: Comparison between the relative contributions of quark and neutrino matrix elements. The square areas stand for the square of the corresponding matrix element.

1.2.2.1 Neutrino Dirac masses

In the SM, fermions are Dirac particles, meaning particles and anti-particles are different. Their masses arise with the Higgs mechanism, through the coupling of left- and right-handed fields with the Higgs doublet. One can imagine the same mechanism arises for neutrinos.

In the SM, only left handed leptons participate in the charged weak interaction. As it is the only force through which neutrinos interact, only the left-handed component is described in the SM for neutrinos. Then, adding a Dirac term in the Lagrangian comes with introducing a right-handed chiral neutrino field, so-called sterile neutrino. They are named that way in order to distinguish them from known left-handed active neutrinos.

Dirac spinors

In the Standard Model, fermions are described by Dirac quantised fields $\psi(x)$, 4-component spinors which are a solution of the Dirac equation,

$$(i\partial\!\!\!/ - m)\psi(x) = 0\,, \tag{1.6}$$

with m the mass of charged leptons. $\partial\!\!\!/ \equiv \gamma^\mu \partial_\mu$ where there is an implied summation over the values of the twice-repeated index $\mu = 0, 1, 2, 3$, and ∂_μ is the 4-gradient. We can describe a Dirac field in term of chiral fields as

$$\psi = \psi_R + \psi_L\,, \tag{1.7}$$

with ψ_R and ψ_L the eigenvectors of the γ^5 chirality projector matrix. ψ_R and ψ_L are called Weyl spinors. Then the Lagrangian for a free fermion field is written as

$$\mathcal{L} = (\overline{\psi_R} + \overline{\psi_L})(i \overleftrightarrow{\partial\!\!\!/} - m)(\psi_R + \psi_L)\,. \tag{1.8}$$

It results from Eqs. (1.6) and (1.7) that ψ_R and ψ_L have independent kinetic terms, but coupled mass terms:

$$i\gamma^\mu \partial_\mu \psi_L = m\psi_R\,, \tag{1.9}$$
$$i\gamma^\mu \partial_\mu \psi_R = m\psi_L\ . \tag{1.10}$$

Consequently, the two chiral component fields are independent only if $m = 0$.

Dirac mass term

Charged leptons are massive in the SM with the Dirac mass term in the Lagrangian:

$$\mathcal{L}_Y^l = -\frac{v}{\sqrt{2}}\,\bar{l}_L\, Y^l\, l_R + h.c.\,, \tag{1.11}$$

where Y^l is the Yukawa matrix for charged leptons, and v is the vacuum expectation value (vev) for the Higgs field. In the SM Lagrangian, there is no mass term for neutrinos, and the lepton Yukawa couplings can be diagonalised without leading to flavour violation in charged lepton currents. Thus the lepton flavour is conserved in the SM.

In the Standard Model, neutrinos only undergo weak interactions. But weak interactions are described by the $SU(2)_L$ group, whose elements act only on left-handed chiral components of the fermion fields. So weak interaction "see" only the LH components of fields. If one goes beyond the SM, one can add a right handed neutrino ν_R, singlet under all gauge interactions ($SU(3)_C \times SU(2)_L \times U(1)_Y$ gauge groups). In this case, and as occurred for the quark and charged lepton sectors, neutrino masses can be generated by the Higgs mechanism, with a Dirac mass term:

$$\mathcal{L}_Y^\nu = -\frac{v}{\sqrt{2}}\,\overline{\nu}_L\, Y^\nu\, \nu_R + h.c.\,. \tag{1.12}$$

Thus to have a Dirac mass term in the Lagrangian, we need to introduce right handed neutrinos ν_R, called sterile neutrinos, because they do not interact through

weak interaction, unlike active neutrinos. If neutrinos and leptons are both massive, one cannot have Y^ν and Y^l simultaneously diagonal. Then the leptonic charged currents are not diagonal anymore, leading to lepton flavour violation. That leads to new processes including neutrino oscillations.

It is important to notice that for Dirac neutrinos, and even if their masses are described by the same mechanism responsible for all other SM fermion masses, the corresponding Yukawa couplings are extremely tiny, many orders of magnitude below Y^l and Y^q (the Yukawa matrix for quarks).

1.2.2.2 Neutrino Majorana masses

Majorana neutrinos

As we have seen in the previous sub-section, 4-component Dirac spinors are used to describe fermion fields. As Eqs. (1.9) and (1.10) are coupled, we could derive one simple expression if we find a link between ψ_R and ψ_L. In the 1930's Ettore Majorana suggested such a link by writing $\psi_R = C\overline{\psi}_L^T$, where C is the charge conjugation matrix and $\overline{\psi} = \gamma^0\psi$. Therefore $C\overline{\psi}_L^T$ is right-handed. We thus have the Majorana condition for fields

$$\psi = C\overline{\psi}^T \,, \tag{1.13}$$

since we have the chiral description for fermion fields in Eq. (1.7). With this condition, fermion fields are now described by a 2-component spinor. Thus a Majorana field has half the number of degree of freedom of a Dirac field. As $C\overline{\psi}_L^T$ is equivalent to ψ_L^C [5], the Majorana condition in Eq. (1.13) can be written as $\psi = \psi^C$. This further implies that a Majorana particle is its own antiparticle. Therefore, Majorana and Dirac particles are fundamentally different particles.

Majorana mass term

An effective field theory (EFT) is an "approximation" of a more general theory. It is used when a physical process is studied at such low energies (or long distances) that we cannot probe the underlying phenomenon that occurs (one says that the heavy fields at the origin of such interactions are "integrated out"). Fermi first described the weak interaction of beta decay with an EFT, when only leptons and hadrons were known. This so-called Fermi theory describes a contact interaction between 4 SM fields. In a more general manner, an effective Lagrangian, which generalises the SM one, has an infinite number of terms as

$$\mathcal{L}_{eff} = \mathcal{L}_{SM} + \sum_d \frac{1}{\Lambda^{d-4}} C^d O^d \,, \tag{1.14}$$

with $d > 4$. C represents the couplings at the effective vertex, and O is an effective non-renormalisable operator with a dimension above 4, which contains only SM fields. For the neutrino case, we want to write a mass term involving only SM fields, that means with the only left-handed neutrino field ν_L. The operator with the lowest dimension - which respects the SM symmetries - to describe neutrino

masses in the SM (without RH neutrinos) is a dimension-5 operator, called the Weinberg operator, which can be represented as in Fig. 1.4 and defined as

$$\mathcal{L}_5 = \frac{1}{2}\frac{g^{eff}}{\mathcal{M}}(\overline{L}_L^c \sigma^2 \phi)(\phi^T \sigma^2 L_L) + h.c.\,, \tag{1.15}$$

where g^{eff} is a dimensionless coefficient corresponding to a new effective coupling and σ the Pauli matrices. L_L is defined by Eq. (1.1) and ϕ represents the Higgs field. In Eq. (1.15), the coefficient C is here identified with $g^{eff}/2$, and O is represented by the [LH][LH] operator. This Lagrangian respects all the SM symmetries, except for the total lepton number conservation. After the electroweak symmetry breaking, the following Lagrangian stands for the neutrino fields

$$\mathcal{L}_5 = \frac{1}{2}\frac{g^{eff} v^2}{\mathcal{M}}\overline{\nu}_L^c \nu_L + h.c.\,, \tag{1.16}$$

where $\mathcal{M}$ denotes a mass scale at which new degrees of freedom, corresponding to new physics, arise. A Majorana mass term for neutrinos can be defined as

$$m_\nu = \frac{g^{eff} v^2}{\mathcal{M}}\,. \tag{1.17}$$

The dimension-5 operator in Eq. (1.15) is not renormalisable. Nevertheless, it is natural to think that actual SM theory is not the final theory, but an effective theory, as a reminiscence of a more complete one. Neutrino masses can then be seen as a low energy manifestation of this physics beyond the Standard Model. There exist many other higher dimension operators, for example, the Fermi operator is a dimension-6 effective operator, as are the operators responsible for charged lepton flavour violation. Notice that the higher the dimension is, the harder is the observation of the corresponding new physics effects.

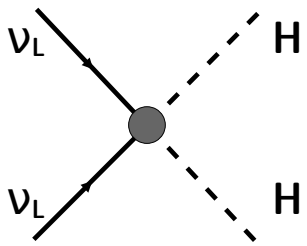

Figure 1.4: Weinberg operator diagram. The grey circle pictures a new physics interaction.

1.2.2.3 Neutrino mass term

In the two previous sub-sections the Dirac and Majorana nature of neutrinos were reviewed. Assuming a right-handed chiral field exists, it is possible to combine the Dirac and Majorana descriptions. A Dirac-Majorana mass term is derived for one generation of neutrinos, for the minimal model where an additional right-handed neutrino is added to the particle content.

Dirac-Majorana mass term

After Eq. (1.12), a Dirac mass term for neutrinos in the Lagrangian can be defined as

$$\mathcal{L}_D = -m_D \overline{\nu}_L \nu_R + h.c.\,, \tag{1.18}$$

with $m_D = \frac{v}{\sqrt{2}} y^\nu$ in the case of one generation of neutrinos, where y^ν embeds the Yukawa coupling. In addition, one can define a Majorana mass term for the right-handed neutrino field as

$$\mathcal{L}_R = \frac{1}{2} m_R \overline{\nu}_R^c \nu_R + h.c.\,, \tag{1.19}$$

with m_R defined in the same manner as in Eq. (1.17). Thus, in general, it is possible to have a Dirac-Majorana mass term in the Lagrangian:

$$\mathcal{L}_{D+M} = \mathcal{L}_D + \mathcal{L}_R = -m_D \overline{\nu}_L \nu_R + \frac{1}{2} m_R \overline{\nu}_R^c \nu_R + h.c.\,. \tag{1.20}$$

This term can be re-written as

$$\mathcal{L}_{D+M} = \frac{1}{2} n_L^T C^\dagger \mathbb{M} n_L + h.c.\,. \tag{1.21}$$

with $n_L = (\nu_L \nu_R^c)^T$, and the non-diagonal matrix

$$\mathbb{M} = \begin{pmatrix} 0 & m_D \\ m_D & m_R \end{pmatrix}. \tag{1.22}$$

For one generation of neutrinos, $\mathbb{M}$ is a (2×2) matrix. In the more general case of three generations, m_D and m_R are (3×3) diagonal matrices. The matrix $\mathbb{M}$ has to be diagonalised in order to have masses for ν_R and ν_L. $\mathbb{M}$ is diagonalised by $U^T \mathbb{M} U$ with U the mixing matrix from interaction to mass basis

$$U = \begin{pmatrix} \cos\theta & \sin\theta \\ -\sin\theta & \cos\theta \end{pmatrix} \begin{pmatrix} \eta_1 & 0 \\ 0 & \eta_2 \end{pmatrix} \tag{1.23}$$

with η_1 and η_2 two phases called Majorana phases, ensuring that masses, eigenvalues of $\mathbb{M}$, are positive. Thus, after diagonalisation, we have the two masses

$$m_{1,2} = \frac{1}{2} \left(m_R \mp \sqrt{m_R^2 + 4 m_D^2} \right) \eta_{1,2}^2\,, \tag{1.24}$$

with $\eta_1 = i$ and $\eta_2 = 1$. Here we note the role of Majorana phases: η_1 guarantees the positiveness of the m_1 solution. Other models, including a Majorana mass term m_L for the ν_L field exist, and allow to describe pure Dirac or pure Majorana conditions.

See-saw mechanisms

The Standard Model forbids a mass term for the ν_L field but predicts nothing for the ν_R field. Considering the case were $m_D \ll m_R$ (and $m_L = 0$) allows to

explain how neutrinos acquire their small neutrino masses, through the see-saw mechanism. Indeed, the two mass eigenstates can be re-written as

$$m_1 \simeq \frac{m_D^2}{m_R} \qquad \text{and} \qquad m_2 \simeq m_R \,. \tag{1.25}$$

If large value is considered for m_R and a small one for m_D, the light neutrino has a mass m_1 corresponding to the observed active one, while the heavy neutrino has a mass m_2 and corresponds to the sterile singlet. This realisation of the see-saw mechanism is the best known, but others exist.

To introduce a Weinberg operator, leading to a Majorana mass term in the Lagrangian, one can consider the most general form $[LHLH]$, composed of Higgs fields H and lepton fields L, and try to combine it in order to have gauge invariant operators.

- It is possible to combine lepton and Higgs fields to have an $SU(2)$ fermion singlet. The corresponding Feynman diagram is represented in Fig. 1.5a. This realisation of the see-saw mechanism was already presented above, where one RH neutrino field gives rise to a mass for one LH neutrino field. In that case, the addition of three RH fields to the model would be sufficient to give masses to the three active neutrinos.

- We can also consider a combination giving a heavy scalar triplet $\xi = (\xi^{++}, \xi^{+}, \xi^{0})$. The corresponding Feynman diagram is presented in Fig. 1.5b. This is a mechanism which does not require right-handed neutrinos.

- The last way to combine lepton and Higgs fields in order to have a gauge invariant Lagrangian consists in introducing a fermionic triplet $\Sigma = (\Sigma^{+}, \Sigma^{0}, \Sigma^{-})$, not to be confused with the baryon of the same name. The Feynman diagram is pictured in Fig. 1.5c.

These three possibilities are in fact the only possible realisations to obtain the effective Weinberg operator, using only renormalisable interactions. They correspond to the so-called type I [6], II [7] and III [8] seesaw mechanisms, respectively.

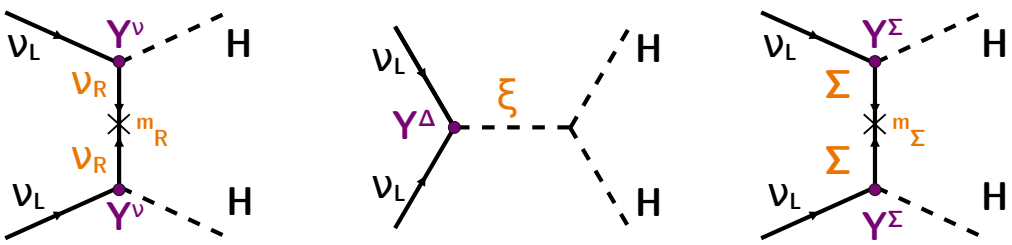

(a) See-saw type I. (b) See-saw type II. (c) See-saw type III.

Figure 1.5

1.2.3 Double beta decays

Even though it is not protected by a symmetry, the total lepton number is conserved in the SM. If the neutrino is found to be a Majorana particle it could open leads for the explanation of lepton number violation, the small masses of the neutrinos through the see-Saw mechanism and the matter/antimatter asymmetry in the Universe through Leptogenesis. Should neutrinos be Majorana particles, their mass term leads to lepton number violation (LNV), with $\Delta L = 2$. The best known process able to probe LNV is neutrinoless double beta decay [9].

Standard double beta decay

Let us first introduce the double beta decay proposed by Goeppert-Mayer in 1935 [10] as

$$(A, Z) \rightarrow (A, Z+2) + 2e^- + 2\overline{\nu}_e \,, \tag{1.26}$$

describing two simultaneous β decays of two nucleons of the same nucleus. This decay is physically possible for nuclei with an even-even number of nucleons, for whose a simple beta decay would not be favourable: the energy of the daughter nucleus would be higher than the parent one. In some cases (as the ^{48}Ca nucleus) the simple β decay is suppressed because of transition spin considerations. This transition is strongly suppressed which makes it the rarest known nuclear decay (see Fig. 1.6). It is allowed by the Standard Model for 35 isotopes, and despite its rarity, has already been observed for numerous of them like ^{100}Mo, ^{82}Se, ^{136}Xe and ^{76}Ge, with typical half-lives ranging from 10^{18} to 10^{24} years. The Feynman diagram illustrating this process is given in Fig. 1.7.

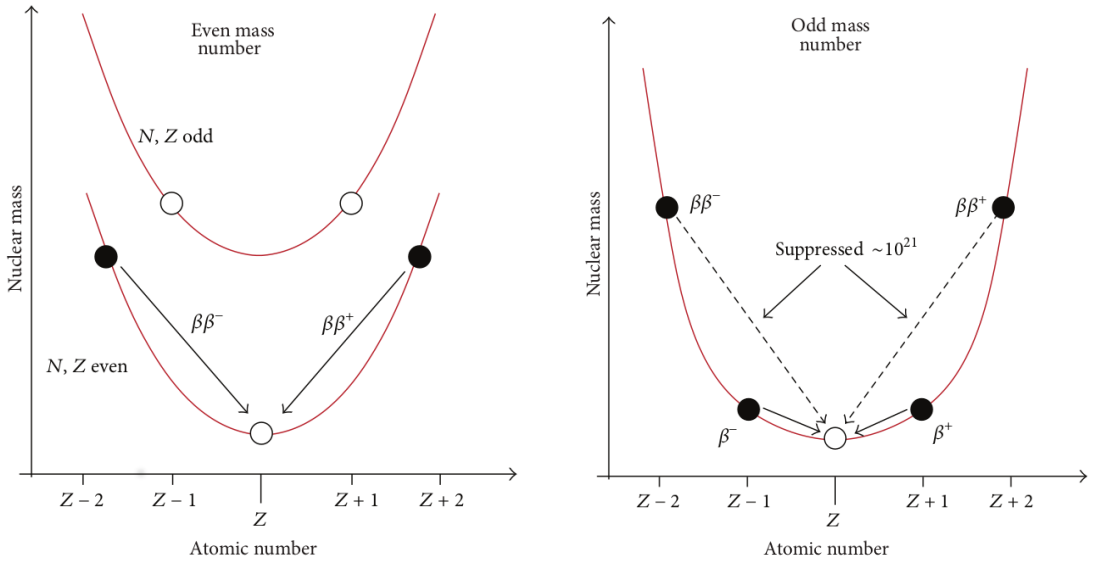

Figure 1.6: Nuclear mass as a function of the atomic number Z in the case of an isotope with A even (a) and A odd (b). Adapted from [11].

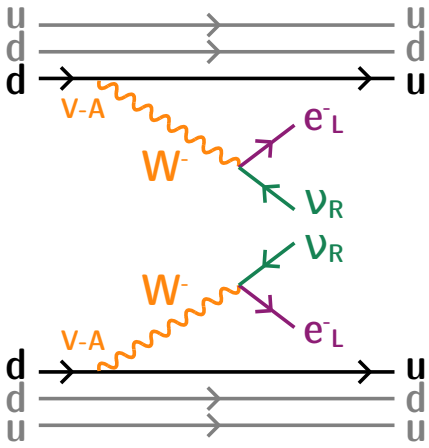

Figure 1.7: Standard double beta decay.

Neutrinoless double beta decay

In 1939, Furry [12] proposed the double beta decay without neutrino production as

$$(A, Z) \rightarrow (A, Z + 2) + 2e^{-} , \tag{1.27}$$

in which two neutrons simultaneously decay into protons.

The existence of such a decay would have deep implications for various physics research. Firstly, as neutrinos are not emitted, this process implies the violation of the total lepton number by 2 units, thus making it forbidden in the SM. However, the lepton number conservation results from an accidental symmetry breaking of the SM, and thus its violation would not necessarily imply Physics beyond the Standard Model. But more than the LNV, the $0\nu\beta\beta$ would violate also the baryon - lepton number (B-L) which, on the contrary, is a fundamental symmetry of the SM. Hence such observation would have major contribution for theories trying to explain the matter/antimatter asymmetry of the Universe. Moreover, the $0\nu\beta\beta$ process is allowed only if neutrinos are massive Majorana particles. Therefore, the observation of this decay would point to the existence of a process that violates a fundamental symmetry of the Standard Model of Particle Physics, and would allow to establish the nature of neutrinos.

At the moment, no experiment has observed $0\nu\beta\beta$ processes, but various experiments, of which a non-exhaustive list is given in Sec. 1.3, have lead to precise limits on $0\nu\beta\beta$ half-life of $10^{25} - 10^{26}$ years. The future generation of $0\nu\beta\beta$ experiment is currently under construction.

The absence of neutrino emission, if detected experimentally, would prove the Majorana nature of the neutrino. The underlying mechanism through which the neutrinoless double beta decay would occur is not known, and several theories have been developed.

- Higher dimensional operators: the dimension-5 Weinberg operator presented above is the lowest dimension operator that can be built for the mass of Majorana. In addition, it is possible to consider higher dimension operator (dimension 6 and 9 for instance), that are effective and non-renormalisable, respecting the gauge symmetry $SU(3)_C \times SU(2)_L \times U(1)_Y$.

- Heavy neutrino exchange considers the case where a heavy RH neutrino is exchanged during the $0\nu\beta\beta$ decay. This was historically the first case to be considered, including a dimension-9 operator, with constraints on the heavy neutrino mass with the mixing between left-handed neutrinos and the heavy neutrino.
- Right-handed currents include new RH gauge bosons W_R of a new $SU(2)_R$ gauge group. The corresponding operator would be of dimension-9 and highly suppressed, by 4 powers of the masses of the new gauge bosons.

In Fig. 1.8 is given the Feynman diagram of the neutrinoless double β decay for the light Majorana neutrino exchange realisation.

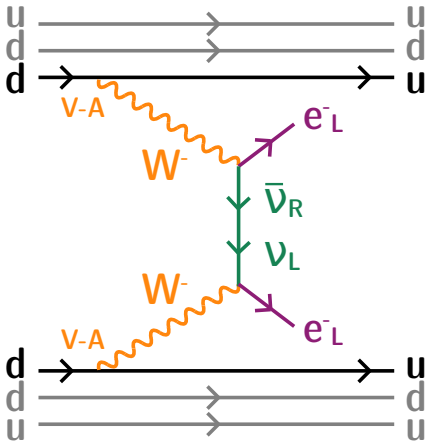

Figure 1.8: Neutrinoless double beta decay through light Majorana neutrino exchange.

Experimental search for $0\nu\beta\beta$

One of the experimental observable of the double β decays is the total energy spectrum of the 2 emitted electrons, given in Fig. 1.9. The $2\nu\beta\beta$ decay emits 4 leptons, the two electrons having an energy continuum between 0 and $Q_{\beta\beta}$, the total available energy of the reaction. In the case of the $0\nu\beta\beta$ decay, the two electrons would bring the total energy of the reaction, thus the expected signature would be an energy peak at $Q_{\beta\beta}$.

If existing, the $0\nu\beta\beta$ decay would be an extremely rare process. The decay rate of the light Majorana exchange is given by:

$$(T^{0\nu}_{1/2})^{-1} = g_A^4 G^{0\nu} |M^{0\nu}|^2 \left| \frac{m_{\beta\beta}}{m_e} \right|^2 . \tag{1.28}$$

where $G^{0\nu}$ is the phase space factor embedding the influence of the Coulomb field of the daughter nucleus on the emitted electrons/positrons. $M^{0\nu}$ is called the nuclear matrix element embedding the nuclear structure effects of the decaying nucleus. $m_{\beta\beta}$ is the effective neutrino mass defined as

$$\langle m_{\beta\beta} \rangle = \left| \sum_{i=1...3} m_i U_{ei}^2 \right| , \tag{1.29}$$

is summed over the three mass eigenstates. This effective mass depends on the U_{PMNS} matrix elements given in 1.5, and thus is a function of the CP violating phases and of the mass ordering.

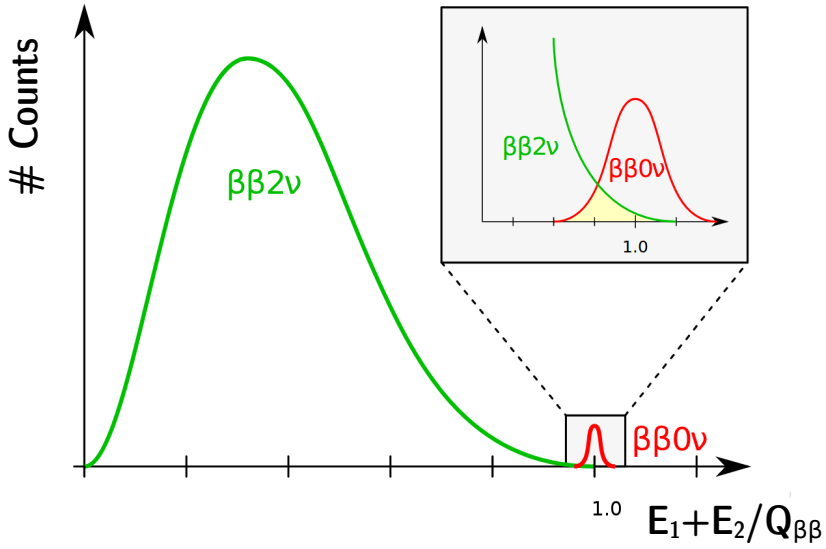

Figure 1.9

1.3 $0\nu\beta\beta$ experimental status

1.3.1 Experimental design criteria

As no neutrinos are emitted in a $0\nu\beta\beta$ decay, the minimal observable in direct searches for $0\nu\beta\beta$ decay is the total energy of the two emitted electrons. Depending on experiment designs and purposes (detailed in Sec. 1.3.2), individual electron energies and tracks also represent interesting observables. The signature of a $0\nu\beta\beta$ signal is an excess of events, compared to the expected background noise, in the total energy spectrum, near the $Q_{\beta\beta}$ released energy. How large is this peak depends on the energy resolution of the detector. Research for this signal involves optimising a *region of interest* (ROI), also depending on the energy resolution. The total number of events $N^{0\nu}$ occurring in the ROI and in the measurement time t, for a detector with an detection efficiency ϵ, using a source isotope of W atomic molar mass and a isotopic abundance, is defined as

$$N^{0\nu} = \ln(2)\frac{\mathcal{N}_A}{W}\left(\frac{a\epsilon Mt}{T^{0\nu}_{1/2}}\right), \tag{1.30}$$

where $\mathcal{N}_A$ is the Avogadro number. If no excess of events is observed, the limit set on the $0\nu\beta\beta$ decay half-life is

$$T_{1/2}^{0\nu,\lim} = \ln(2)\frac{\mathcal{N}_A}{W}\left(\frac{a\epsilon Mt}{N_{\text{exc}}}\right), \tag{1.31}$$

N_{exc} being the number of $0\nu\beta\beta$ events excluded at a given confidence level in the ROI. Then, this sensitivity to the $0\nu\beta\beta$ decay would depend on the number of total counts in the ROI, some of them possibly being background events:

$$T_{1/2}^{0\nu,\lim} \propto \begin{cases} aM\epsilon t & \text{if no background is expected,} \\ a\epsilon\sqrt{\frac{Mt}{B\Delta E}} & \text{with background.} \end{cases} \tag{1.32}$$

Here B is the background rate usually expressed in counts.keV^{-1}.kg^{-1}.y^{-1} (when normalised to the width of the ROI, the source mass, and the observation time) and ΔE is the energy resolution. The advantage of a background free experiment clearly comes out: the $0\nu\beta\beta$ half life would increase linearly with the time of exposure t (as opposed to $\sqrt{t}$ for an experiment with a large number of background events). Then, it is clear that the control and the discrimination of background is of high priority for such $0\nu\beta\beta$ direct search experiments. We will discuss in Chap. 2 some important point to reduce the backgrounds for the $0\nu\beta\beta$ decay detection. Next to that, the previous expression fixes the choices that experimenters can make in designing a detector. An ideal isotope would have a high natural abundance and would be deployed with the highest mass possible in a detector with a high detection efficiency, a good energy resolution (small ΔE) under low-background conditions (small B). Of all the 35 isotopes capable of disintegrating through $2\nu\beta\beta$, none meets all the previous conditions. Experimenters will then have to find compromises, which are at the origin of the different detection strategies. Detector can ether use an active or passive source. In the first case, the source is also the detection medium (detector technologies detailed in Sec. 1.3.2.1, 1.3.3 and 1.3.5). In the second case, the source is decoupled from the detection part of the experiment (see Sec. 1.3.4 and 1.3.6). In the next section, we provide a review of the current and future experiments that aim to discover the neutrinoless double beta decay.

1.3.2 $0\nu\beta\beta$ direct search experiments

1.3.2.1 Semiconductors

Various semiconductor technologies are employed in the detection of $0\nu\beta\beta$ decay. The ^{76}Ge $\beta\beta$ emitter ($Q_{\beta\beta}$ = 2039 keV) is historically important as it has been adopted since the 1960s in $0\nu\beta\beta$ decay searches, acting as active source, which enhances the detection efficiency. ^{76}Ge-enriched high purity Germanium detectors (HPGe) offer both high energy resolution and extremely high radiopurity (as impurities are removed in the crystal growing process). These characteristics allow, once external background contribution is minimised, to reach high sensitivity on $0\nu\beta\beta$ decay, which makes this category of detectors one of the most promising for ton-scale experiments. Since the last generation (IGEX and Heidelberg-Moscow),

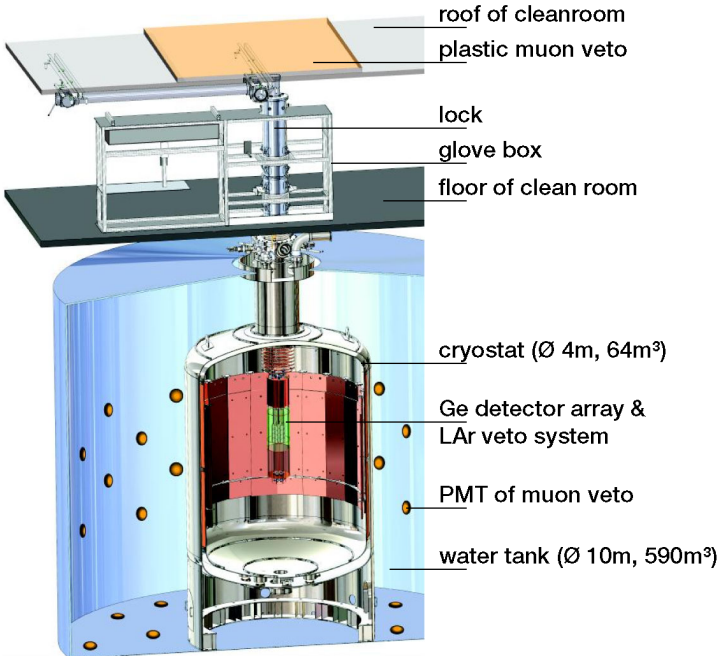

Figure 1.10: Scheme of the GERDA experiment.

HPGe detectors had been improved to reach an ultra low background rate, making way for the current generation of $0\nu\beta\beta$ detectors – GERDA, MAJORANA demonstrator and LEGEND.

GERDA experiment (GERmanium Detector Array) is located at the Laboratori Nazionali del Gran Sasso (LNGS), Italy. GERDA phase I was running from 2011 to 2013 with 17.8 kg of enriched active source detectors from the HEIDELBERG-MOSCOW and IGEX experiments. Its first aim was to put to the test the controversial result of HEIDELBERG-MOSCOW experiment given in 2001, announcing the first evidence for $0\nu\beta\beta$ signal at a 4.2σ confidence level. With an exposure of 21.6 kg.y, the absence of signal in the GERDA-I experiment refuted the previous result, setting a limit $T^{0\nu}_{1/2} > 2.1\,10^{25}$ y. Since 2015, the GERDA experiment is in the second phase (see Fig. 1.10), with a total of 35.8 kg enriched detectors, 20 kg of which is Broad Energy Germanium (BEGe) detectors that have been deployed for GERDA-II, providing a better energy resolution and pulse shape discrimination. The active source is deployed inside a liquid Argon (LAr) augmented with light sensors, acting as an active external shield as well as a cooling down system. The total is surrounded by a water tank. The aim is to reach a 10^{26} y sensitivity with 100 kg.y exposure, and a background rate less than 10^{-3} counts.keV^{-1}.kg^{-1}.y^{-1}. The underground laboratory of INFN provides 3500 m water equivalent to reduce the external cosmic background. In 2019, a combined analysis for GERDA phases I and II has resulted in a half-life limit of $T^{0\nu}_{1/2} > 9\,10^{25}$ y (90% C.L., sensitivity assuming no signal is $1.1\,10^{26}$), corresponding to an effective neutrino mass of $m_{\beta\beta} < 0.07$-0.16 eV (90% C.L.).

MAJORANA demonstrator is an array of enriched germanium detectors that searched for the $0\nu\beta\beta$ decay of the ^{76}Ge isotope, using High Purity Germanium (HPGe) detectors. The Majorana Demonstrator is located at the Sanford Underground Research Facility (SURF) in Lead, USA. It is composed of 58 HPGe detectors divided into 2 cryostats with 7 strings each. Each string is an assembly of 3, 4 or 5 detectors. The total mass of HPGe crystals is 44.1 kg, 29.7 kg of which is enriched to 88% ^{76}Ge. The observed lower limit is $T^{0\nu}_{1/2} > 2.7 \times 10^{25}$ years at 90% CL [13]. A combined limit from the two Ge-based experiments GERDA and MAJORANA would exceed 10^{26} years.

LEGEND for Large Enriched Germanium Experiment for Neutrinoless Double-Beta Decay. After the encouraging results of the MAJORANA Demonstrator and GERDA, the LEGEND collaboration has been formed to pursue a tonne-scale ^{76}Ge experiment, with discovery potential at a half-life beyond 10^{28} years. The collaboration aim to use existing material from GERDA, especially the cryostat, and perform additional R&D to build the detector.

1.3.3 Bolometers

Bolometers are high energy resolution and high detection efficiency calorimeters operating at low temperatures ($\simeq 10 - 20$ mK), by measuring the heat increase, quantified by phonons, generated by particles interaction in the crystal. This technology provides a good energy resolution of few keV. The crystals are both the source and the detector, which is particularly suitable for $0\nu\beta\beta$ searches, and provides the possibility to build large-scale experiments. As the two electrons topology is not available, analyses of the pulse shapes can be performed in order to discriminate the signal from the electronics noise and the natural radioactivity events.

CUORE for Cryogenic Underground Observatory for Rare Events, is an experiment based at Laboratori Nazionali del Gran Sasso in Italy. The feasibility of the project has been proved by Cuoricino, the pilot experiment taking data from 2003 to 2008 with 62 TeO2 cryogenic detectors, for a total of 19.75 kg.y exposure, achieving a lower limit of $T^{0\nu}_{1/2} > 2.8 \times 10^{24}$ years at 90% CL. The next step towards the final experiment CUORE was CUORE-0, aiming at improve the background reduction. The data took place from 2013 to summer 2015, showing the α background were reduced by a factor 6. The CUORE detector consists of an array of 988 TeO2 crystals arranged in a cylindrical structure of 19 towers. The first results of the CUORE experiment had been published in 2018, where no evidence for $0\nu\beta\beta$ were found. Combining their results with the earlier experiments Cuoricino and CUORE-0, a lower limit of $T^{0\nu}_{1/2} > 1.5 \times 10^{25}$ years at 90% CL were achieved.

CUPID for CUORE Upgrade with Particle IDentification, uses the expertise acquired with the CUORE facility, with a background level improved by a factor 100 as the particle identification is a powerful tool for background rejection. This

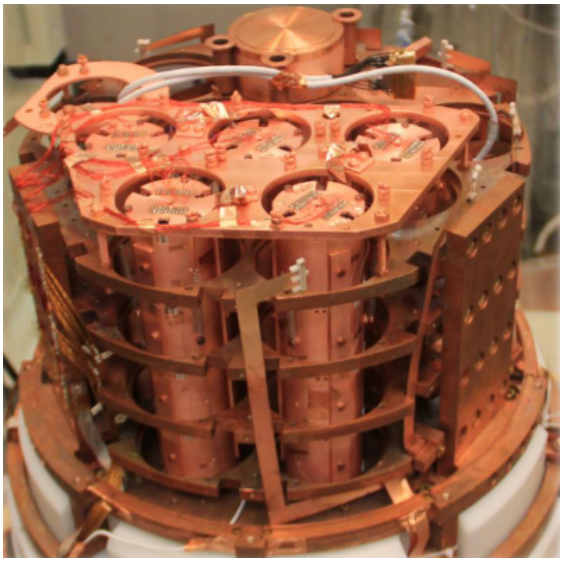

Figure 1.11: Picture of the CUPID-Mo project.

technology uses scintillating bolometers, and is based on the principle that different particles produce different amount of light, providing a good discrimination between γ and α background events. The first CUPID-0 detector uses 24 crystals enriched at 95% with ^{82}Se, for a total mass of 5.17 kg, coupled with 31 Germanium light detectors. It is hosted in the CUORE-0 cryostat at LNGS. With an exposure of 9.95 kg.y, the CUPID-0 collaboration presented the first results with a lower limit of $T^{0\nu}_{1/2} > 3.5 \times 10^{24}$ years at 90% CL. These first results are encouraging for the next CUPID project, showing a high α rejection. The ^{82}Se material is however not suitable for CUPID, making the crystal growth complicated and showing a high internal contamination in natural isotopes. The next project CUPID-Mo was commissioned in 2019 and is already taking data at Laboratoire Souterrain de Modane in France, with 210 g of $Li_2^{100}MoO_4$ crystals, divided into 5 towers of 4 modules each (see Fig. 1.11). Preliminary results have been presented and show a high energy resolution (about 5 keV FWHM), a good γ/α discrimination, and a high internal radiopurity, demonstrating that the CUPID technology is ton-scalable.

1.3.4 Time projection chambers

Time Projection Chambers (TPC) detectors use a medium producing two ways to measure the electron energies: a *scintillation* (ultra-violet light) prompt signal, and a *ionisation* delayed signal. When a particle crosses the detector, a scintillation light is emitted, the energy of the scintillation peak depending on the medium. Scintillation photons, travelling at speed of light in the medium, are detected by photo-sensors, giving the *zero-time* of the event. The crossing particle ionises the medium all along its way, creating electrons drifting to a collection system (an electric field is applied between cathode and anode), allowing the precise measurement of the electron production location in a 2D plane. The drift time measurement gives access to the third coordinate of the interaction point.

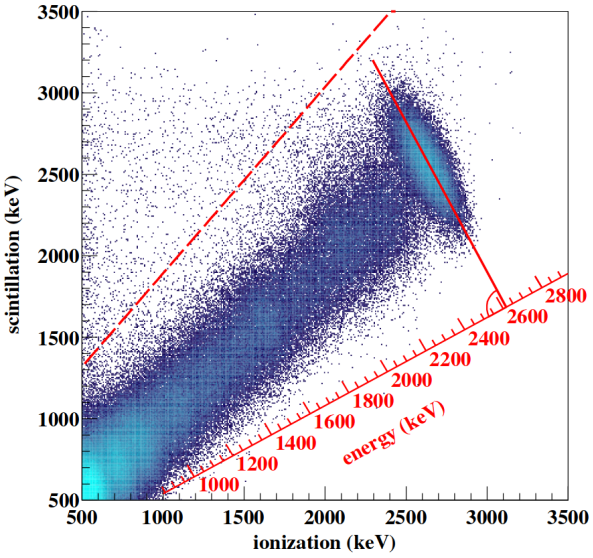

Figure 1.12: Scintillation light energy as a function of ionisation energy.

Therefore, combining the two consecutive signals allows precise position and energy reconstruction. A discriminating observable is the ionisation-to-scintillation ratio (see Fig. 1.12) as it provides particle discrimination between α particles (low ratio) and γ radiations and β particles (high ratio). For $0\nu\beta\beta$ searches, ^{136}Xe-enriched isotope in liquid phase is used, offering a maximal source density (more compact detectors) and a good position resolution. Unfortunately, the energy resolution is worse than that of the gas-phase TPCs detectors[1]. Noble elements are natural radiation detectors, avoiding the need for excess materials that could generate extra radioactive backgrounds. ^{136}Xe-enriched is the only noble element capable to $2\nu\beta\beta$ decay, with $Q_{\beta\beta} = 2457.8$ keV. This isotope has a relatively high natural abundance (9%), can be enriched to highly pure concentrations, and does not have other long-lived radioactive isotopes, making it interesting for large-scale TPCs $0\nu\beta\beta$ experiments.

EXO-200 experiment is a prototype of the Enriched Xenon Observatory (EXO) project, currently operating in a room under an overburden of 1624 m.w.e, at the Waste Isolation Pilot Plant (WIPP), USA. The detector is shaped as a cylinder, with two back-to-back cylindrical TPCs. A high negative voltage grid cathode holds at the mid plane of the detector (40 cm diameter), and two anodes are located on both sides, at ground potential. A cross-section of the detector is displayed in Fig. 1.13. With 110 kg of enriched ^{136}Xe in liquid phase (the detector is held at 167 K in a cryogenic bath), the phase I of this TPC detector has measured for the first time the Xenon $2\nu\beta\beta$ decay with $T^{0\nu}_{1/2} = 2.165\times10^{21}$ y. Between phase I and IIa, the detector was upgraded with improved low-noise electronics, a Radon suppression system, and the impurities contents of the Xenon were reduced by a factor ten. The current detector performance shows an energy resolution of 2.90% (FWHM)

[1]Two-phase liquid-Xenon detectors are developed for Dark Matter searches and could be exploited for $0\nu\beta\beta$ direct searches with the DARWIN project.

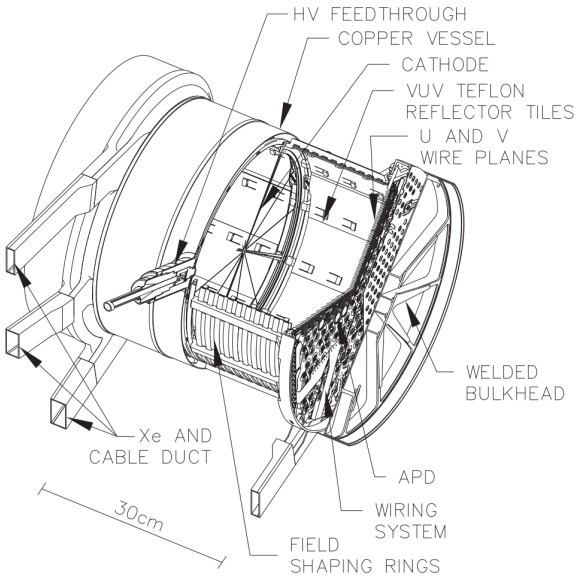

Figure 1.13: Cross-section of the EXO-200 TPC detector

at the decay Q-value and a background rate of 1.6×10^{-3}counts.keV^{-1}.kg^{-1}.y^{-1}. EXO-200 phase IIa data placed a new limit of $T^{0\nu}_{1/2} > 1.8 \times 10^{25}$ y (90% C.L.). The final analysis allowed to reach 5.0×10^{25} years at 90% CL with a 234.1 kg.y exposure [14].

nEXO is the successor of EXO-200 searching for the $0\nu\beta\beta$ decay of ^{136}Xe with a target half-life sensitivity of $\sim 10^{28}$ years using 5×10^3 kg of enriched liquid-xenon in a time projection chamber. This limit would be reached by using an increased mass of enriched ^{136}Xe, and an active R&D program, aimed primarily at improving the active medium homogeneity.

NEXT for Neutrino Experiment with a Xenon TPC is searching for the $0\nu\beta\beta$ decay of ^{136}Xe isotope at the Canfranc underground laboratory in Spain [15]. This technology uses high-pressure gaseous Xenon at 15 bar with using electroluminescence to amplify the signal (HPXe). The gas medium allows to obtain longer particle tracks than with liquid Xenon and the ability to reconstruct the trajectory of the two electrons emitted, contributing to the suppression of backgrounds. The NEXT-100 project, which deploys 100 kg of enriched Xenon, aims to demonstrate the feasibility of such an experiment and its usefulness for the $0\nu\beta\beta$ searches.

PandaX-III also searches for the $0\nu\beta\beta$ of ^{136}Xe with a high pressure gas TPC (10 bar). It is installed at the China Jin Ping underground Laboratory (CJPL) and contains 200 kg of 90% enriched ^{136}Xe. The previous PandaX-II detector is a dark matter direct detection experiment.

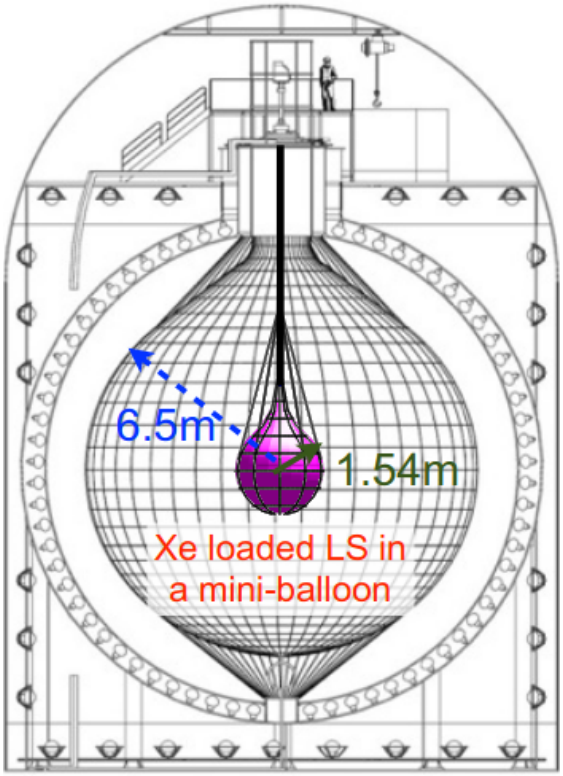

Figure 1.14: Sketch of the KamLAND-ZEN detector.

1.3.5 Liquid scintillators

In this section are presented two large-scale detectors, first designed to measure the solar neutrino oscillations. By adding $\beta\beta$ isotopes to their large detection volume, they now both aim at searching for the $0\nu\beta\beta$ decay. The main drawbacks of these detectors are the poor energy resolution as well as the absence of event topology reconstruction. This is nevertheless compensated by the high exposure, as they both contain the highest quantities of $\beta\beta$ isotopes, allowing to reach high $T^{0\nu}_{1/2}$ limits. We also review two new liquid scintillator technologies.

KamLAND-ZEN for Kamioka Liquid Scintillator Antineutrino Detector - Zero Neutrino Double Beta Decay Search, is located in the underground neutrino detection facility in Japan. It uses the original design of KamLAND detector that precisely measured 2 cycles of neutrino oscillations. This detector searches for the $0\nu\beta\beta$ decay of the ^{136}Xe isotope, by installing a mini-balloon at the centre of KamLAND (Fig. 1.14). The chosen isotope, enriched at 91%, is dissolved in a liquid scintillator, and a purification method is well-established for both of them, allowing to reach low internal background levels. The first phase, the KamLAND-Zen 400 project, was already terminated and its latest limit for half life of $0\nu\beta\beta$ is $T^{0\nu}_{1/2} > 1.07 \times 10^{26}$ years at 90% CL [16]. This result confirmed the feasibility of such high-scale technology, and KamLAND-Zen 800 has started taking data in January 2019 with 745 kg of ^{136}Xe, planning a ~ 5 years data acquisition.

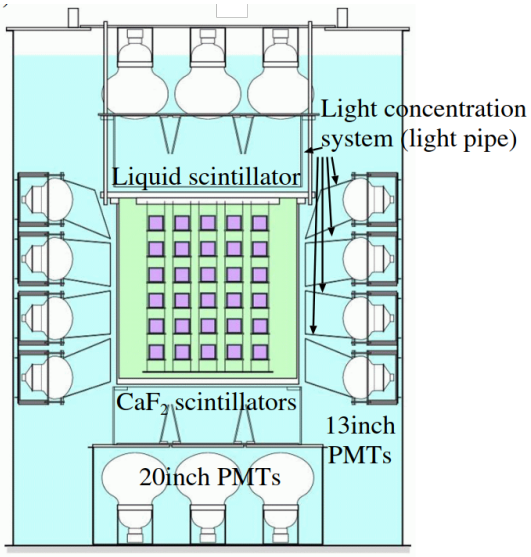

Figure 1.15: Sketch of the CANDLES detector.

SNO+ is an experiment using the existing SNO detector located in SNOLAB (6000 m.w.e.) in Canada, by replacing the water volume with a liquid scintillator. This offers the possibility to search for the $0\nu\beta\beta$ decay by loading 800 kg of ^{130}Te isotope into 780 tonnes of scintillating solution. The huge quantity of isotope loaded into SNO+ gives a significant advantage over other $0\nu\beta\beta$ experiments. This technology aims at reaching a lower limit on the $0\nu\beta\beta$ half-life of 9×10^{25} years after 5 years.

ZICOS is a new experiment using a liquid scintillator loaded with enriched zirconium. The goal is to use 865 kg of ^{96}Zr enriched at 50% to reach a sensitivity of $\sim 1 \times 10^{27}$ years. This sensitivity would be achieved by an efficient ^{208}Tl background reduction using the information of Cherenkov light.

CANDLES is a project searching for $0\nu\beta\beta$ with ^{48}Ca installed at the Kamioka underground laboratory. The chosen isotope has an advantage of the highest $Q_{\beta\beta}$ of 4.27 MeV. The 96 CaF2 scintillator detectors, for a total mass of 305 kg, are immersed in a liquid scintillator. Scintillation light from the CaF2 scintillators and from the liquid scintillator are measured by 62 photomultiplier tubes (see Fig. 1.15).

1.3.6 Tracking calorimeters

Tracking calorimeters technology, instead of using a *source-as-detector*, employ a passive source shaped as thin source foils of enriched $\beta\beta$ emitters. Sources are placed at the detector centre, surrounded by two trackers allowing for particle identification (between electrons, positrons, γ and α particles) and vertex reconstruction to improve the background rejection. The whole is sandwiched between calorimeters enabling individual particle energy reconstruction. In case of a discovery, this passive source tracking calorimeter technology provides

topological information on angular emissions of the two electrons from $\beta\beta$ decay, making possible to distinguish between underlying mechanisms for $0\nu\beta\beta$ decay.

NEMO for Neutrino Ettore Majorana Observatory was installed in LSM and has taken data from 2003 to 2011 with 7 different $\beta\beta$ isotopes. This detector has set limits on the $0\nu\beta\beta$ half-life of these 7 isotopes between 0.9×10^{19} and 1.1×10^{24} years.

SuperNEMO experiment is a next-generation of detector, inheriting the lineage of the NEMO experiments. It aim at searching for the $0\nu\beta\beta$ decay of several isotopes as ^{82}Se, ^{150}Ndand ^{96}Zr, with about 100 kg of enriched material. The detector will be composed of 20 modules of $\sim$ 5 kg of source each. Giving its low isotope mass, SuperNEMO might not be the first experiment to observe the searched decay, but would identify the underlying mechanism responsible for this decay, thanks to its tracking capabilities. The first module, aiming at demonstrate the scalability of such a technology, is on the commissioning phase, with 6.23 kg of enriched ^{82}Se.

1.3.7 Summary

All expermients esented above aim at searching for the $0\nu\beta\beta$ decay with specific features. Various approaches have been reviewed in this section, and a non-exhaustive list of expermient has been given. The results of the current generation of detectors will make it possible to determine which technologies are the best suited for the search for $0\nu\beta\beta$ decay.

1.4 Conclusion

This chapter presented the questions that are still open around the physics of the neutrino. This particle, discovered relatively late in the history of physics, could allow us to explore physics beyond the Standard Model, and to get closer to a more global theory of physics. Notably, the observation of the $0\nu\beta\beta$ decay would prove that the neutrino is a Majorana particle, while demonstrating that the lepton number is not a symmetry of physics. Beyond the physics of the neutrino, such an observation would have great implications in many fields of physics, and this is why a multitude of experiments are looking for this disintegration. The SuperNEMO detector, on which I worked during my PhD, is one such experiment.

Bibliography

[1] Fermi E. Tentativo di una teoria dei raggi ? *La Ricerca Scientifica*, 1933.

[2] Pontecorvo B. Mesonium and antimesonium. *Soviet Phys. JETP*, 1958.

[3] Fukuda Y. et al. Evidence for oscillation of atmospheric neutrinos. *Phys.Rev.Lett.*, 81:1562–1567.

[4] F. Capozzi et al. Status and prospects of global analyses of neutrino mass-mixing parameters. *Journal of Physics: Conference Series*, 888:012037, sep 2017.

[5] Giunti C. and Kim C. W. *Fundamentals of neutrino physics and astrophysics.* Oxford, 2007.

[6] Minkowski P. $\mu \to e\gamma$ at a rate of one out of 109 muon decays? *Physics Letters B*, 67:421–428, 1977.

[7] Ernest M. Pathways to naturally small neutrino masses. *Physical Review Letters*, 81:1171, 1998.

[8] Marshak R. and Mohapatra R. Invited talk given at orbis scientiae, 14-17 Jan 1980.

[9] Drewes M. The phenomenology of right handed neutrinos. *International Journal of Modern Physics E*, 22, 2013.

[10] Goeppert-Mayer M. Double beta-disintegration. *Physical Review*, 48:512, 1935.

[11] Dell'Oro S. et al. Neutrinoless double beta decay: 2015 review. *Advances in High Energy Physics*, 2016:37, 2015.

[12] Furry W.H. On transition probabilities in double beta-disintegration. *Physical Review*, 56:1184, 1939.

[13] S.I. Alvis et al. Search for neutrinoless double-beta decay in ^{76}ge with 26 kg-yr of exposure from the majorana demonstrator. *Phys. Rev. C*, 100, 2019.

[14] G. et al Anton. Search for neutrinoless double-β decay with the complete exo-200 dataset. *Phys. Rev. Lett.*, 123:161802, Oct 2019.

[15] J.J. et al Gomez-Cadenas. The next experiment. *Phys. Rev. Lett.*, pages 1732–1739, Apr-Jun 2016.

[16] A. Gando et al. Search for majorana neutrinos near the inverted mass hierarchy region with kamland-zen. *Phys. Rev. Lett.*, 117:082503, Aug 2016.

[17] M. Agostini et al. Probing majorana neutrinos with double-β decay. *Science 365*, 1445, 2019.

[18] O. Azzolini et al. First result on the neutrinoless double-β decay of ^{82}Se with cupid-0. *Phys. Rev. Lett.*, 120:232502, Jun 2018.

[19] C. Alduino et al. First results from cuore: A search for lepton number violation via $0\nu\beta\beta$ decay of ^{130}Te. *Phys. Rev. Lett.*, 120:132501, Mar 2018.

[20] J. B. Albert et al. Search for neutrinoless double-beta decay with the upgraded exo-200 detector. *Phys. Rev. Lett.*, 120:072701, Feb 2018.

[21] Chopra A. C0 commissioning results. Internal presentation, 2015.

[22] Cerna C. Tracker review conclusions. Internal presentation, 2014.

[23] Estar database (nist). http://physics.nist.gov/PhysRefData/Star/Text/ESTAR.html.

[24] A. Huber. *Recherche de la nature du neutrino avec le détecteur SuperNEMO : Simulations optiques pour l'optimisation du calorimètre et performances attendues pour le ^{82}Se.* PhD thesis, Université Bordeaux, 2017.

[25] Xcom database (nist). http://physics.nist.gov/PhysRefData/Xcom/html/xcom1.html.

[26] S. Clavez. *Development of reconstruction tools and sensitivity of the SuperNEMO demonstrator.* PhD thesis, Université Paris Sud, 2017.

[27] Garrido X. Bongrand M. Hamamatsu 8" pmt test in magnetic shield. Internal presentation, 2014.

[28] Loaiza P. Source foils measurement with bipo. Internal presentation, 2017.

[29] Perrot F. Radiopurity measurements for 8" pmts and preliminary budget for the sn demonstrator. Internal presentation, 2017.

[30] Arnold R. et al. Technical design and performance of the nemo3 detector. *Nucl. Instrum. Meth. A*, pages 79–122, 2005.

[31] R. Arnold et al. Results of the search for neutrinoless double-β decay in ^{100}mo with the nemo-3 experiment. *Phys. Rev. D*, 2015.

[32] Xin Ran Liu. Radon mitigation strategy and results for the supernemo experiment. IoP APP / HEPP Conference, 2018.

[33] R. Arnold et al. Probing new physics models of neutrinoless double beta decay with supernemo. *Eur. Phys. J. C*, 2010.

[34] R. Arnold et al. Final results on ^{82}se double beta decay to the ground state of ^{82}kr from the nemo-3 experiment. *Eur. Phys. J. C*, 2018.

[35] Cousins D. Feldman G. A unified approach to the classical statistical analysis of small signals. *Phys.Rev.*, pages 3873–3889, 1999.

[36] J. Kotila and F. Iachello. Phase-space factors for double-β decay. *Phys. Rev. C*, 85:034316, Mar 2012.

[37] Dong-Liang Fang, Amand Faessler, Vadim Rodin, and Fedor Šimkovic. Neutrinoless double-β decay of deformed nuclei within quasiparticle random-phase approximation with a realistic interaction. *Phys. Rev. C*, 83:034320, Mar 2011.

[38] A. Chapon. *Mesure des processus de double désintégration bêta du Mo vers l'état excité 0_1^+ du Ru dans l'expérience Nemo3, Programme de R&D SuperNEMO : mise au point d'un détecteur BiPo pour la mesure de très faibles contaminations de feuilles sources.* PhD thesis, Université Caen Basse-Normandie, 2011.

[39] Snow S. A magnetic field map for the tracker. Internal presentation, 2015.

[40] A. Pin. *Recherche de la nature du neutrino via la décroissance double bêta sans émission de neutrinos. Caractérisation et optimisation du calorimètre SuperNEMO et impact sur la recherche de la décroissance du 82Se Développement du premier prototype LiquidO.* PhD thesis, Université Bordeaux-Gradignan, 2020.

[41] A. H. Wapstra G. Audi. The 1995 update to the atomic mass evaluation. *Nucl. Phys. A*, 595:409–480, feb 1995.

[42] R. Arnold et al. Measurement of the $2\nu\beta\beta$ decay half-life of ^{150}nd and a search for $0\nu\beta\beta$ decay processes with the full exposure from the nemo-3 detector. *Phys. Rev. D*, 94, oct 2016.

[43] Nucleid database.

[44] My github page. https://github.com/girardcarillo.